STATISTICAL PHYSICS OF MEMBRANES AND LAMELLAR SYSTEMS

DAVID H. BOAL, *Department of Physics, Simon Fraser University, Burnaby, British Columbia, Canada*

	Introduction	541
1.	**Membranes and Networks**	542
1.1	Fluid Membranes	542
1.2	Polymerized Membranes and Networks	544
1.3	Multilamellar Systems	546
2.	**Elasticity**	546
2.1	Deformations and the Strain Tensor	546
2.2	Elastic Moduli	547
2.3	Bending Resistance	548
2.4	Elasticity and Fluctuations	549
3.	**Flexible Chains**	550
3.1	Ideal Chains	550
3.2	Self-Avoiding Chains	550
3.3	Self-Avoiding Rings	552
3.4	Chain Elasticity	552
4.	**Fluctuating Membranes**	553
4.1	Fluid Membranes	553
4.2	Polymerized Membranes	555
4.3	Membranes under Stress	556
4.3.1	Closed Fluid Membranes	556
4.3.2	Open Membranes at a Wall	556
4.3.3	Planar Membranes under Tension	556
5.	**Systems with Defects**	557
5.1	Percolation Phenomena	557
5.2	Defective Two-Dimensional Networks	557
5.3	Defective Membranes in Three Dimensions	558
6.	**Interactions between Membranes**	558
6.1	Interactions between Rigid Surfaces	558
6.1.1	van der Waals Forces	559
6.1.2	Double-Layer Forces	559
6.1.3	Hydration Forces	559
6.1.4	Steric Interactions	559
6.2	Entropic Repulsion of Fluctuating Membranes	559
6.3	Unbinding Transition	561
	Glossary	561
	Works Cited	561
	Further Reading	562

INTRODUCTION

"Like gold to ayery thinnesse beate"
—John Donne, *A Valediction: forbidding mourning*, 1611

In the nineteenth century, Lord Raleigh speculated that oil spread on water could form a layer only one molecule thick. By spreading a known volume of oil on a calm lake and estimating, by observing reflected light, the area that the oil covered, he was able to determine that the layer had a thickness in the range of 10^{-9} m. Today, we know of many examples of thin sheets, networks, and membranes that occur naturally in biological systems or that can be produced by a variety of physical and chemical means. These membranes and networks are very flexible and have small elastic moduli. For example, the volumetric compression resistance of a protein network in a cell may be more than ten million times smaller than that of a typical liquid.

The properties of highly flexible materials are a natural area of application for statistical mechanics. Many interesting characteristics of rubber, such as the observation first made by John Gough in 1805 that natural rubber contracts when heated, arise from the entropic properties of polymeric chains. The chains in such materials are flexible at the molecular level and possess a large number of equal-energy conformations, or equivalently, have substantial conformational entropy. Statistical mechanics explains Gough's observations by demonstrating that a flexible chain behaves like a spring with a spring

3-527-29300-0/97/$5.00 + .50

constant that increases linearly with temperature.

Viewed as two-dimensional generalizations of one-dimensional chains, membranes show a rich behavior on mesoscopic length scales. Computer simulations argue that *fluid* membranes, with vanishing in-plane shear modulus, exhibit highly convoluted configurations on long length scales, whereas *polymerized* membranes, which resist an in-plane shear, are asymptotically flat. Further, the elastic moduli of membranes are predicted to be wavelength dependent. In their interaction with each other, and with rigid objects such as flat walls, membranes unbind at high temperatures because of thermal undulations.

The study of the elastic and geometrical properties of membranes is a rapidly advancing field with an interplay of experiment, analytical theory, and computer simulation. Insights obtained from each of these physical approaches are contained in the following pages, which also include a short review of some concepts from polymer physics for both comparative and illustrative purposes. Space does not permit the presentation here of the application of statistical mechanics to the phase behavior of surfactant/solvent systems. We describe several of these phases in Sec. 1, where their existence is taken as given, but refer the interested reader to the monographs by Israelachvili (1992), Mouritsen (1988), and Safran (1994) for detailed experimental and theoretical treatments.

1. MEMBRANES AND NETWORKS

1.1 Fluid Membranes

Surface-active agents (or *surfactants*) owe their grease-cutting success to their affinity to both polar and nonpolar solvents. Surfactants are referred to as *amphiphilic*, reflecting their common attraction to otherwise immiscible liquids. Viewed at the molecular level, common soap (sodium stearate) has a long hydrocarbon chain that is attractive to nonpolar liquids such as oil and has a polar carboxylate group at the end of the chain that is attractive to polar liquids such as water; these two interactions are referred to as *hydrophobic* and *hydrophilic*, respectively. The molecular structures of two families of amphiphiles, fatty acids and dual-chain lipids, are illustrated in Fig. 1. Most lipids found in biomembranes have two chains with 16–18 carbon atoms per chain and head groups that are geometrically smaller than the hydrocarbon chains. Some phospholipids, for example, have just a three- or four-segment group (e.g., $-CH_2-CH_2-NH_2$) linked to the carboxylate end of the hydrocarbon chains through a phosphate group ($-PO_4-$) [see Gennis (1989) or Alberts *et al.* (1989) for further details].

While amphiphiles play an important role at interfaces in ternary systems such as oil/water/amphiphile, complex phases are found even in binary systems such as water plus amphiphile. Concentration, temperature, and *p*H are among the conditions that influence the phase structure of binary and ternary systems containing amphiphiles. Among other things, what makes these phases of interest biologically is that the amphiphiles self-assemble into structures with mesoscopic dimensions. Some aspects of the mesoscopic geometry have been interpreted in terms of the molecular geometry of the amphiphile, as we now attempt to demonstrate by example [see Israelachvili (1992) for further details].

Consider first the simple system of water and a single-chain lipid such as a fatty acid. At very low concentrations, the amphiphile dissolves in the conventional manner into the water solvent. In spite of the hydrophobic nature of the amphiphile's hydrocarbon

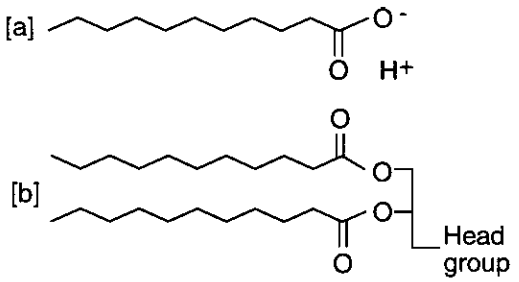

FIG. 1. Molecular structure of two families of amphiphiles. Molecule (a) is a fatty acid, having a single hydrocarbon chain terminating in a carboxylic acid group. Molecule (b) is a dual-chain lipid, with two hydrocarbon chains and a polar head group. In a typical phospholipid, the head group is much smaller than the hydrocarbon chains (e.g., $-PO_4-CH_2-CH_2-NH_2$ for phosphatidyl ethanolamine).

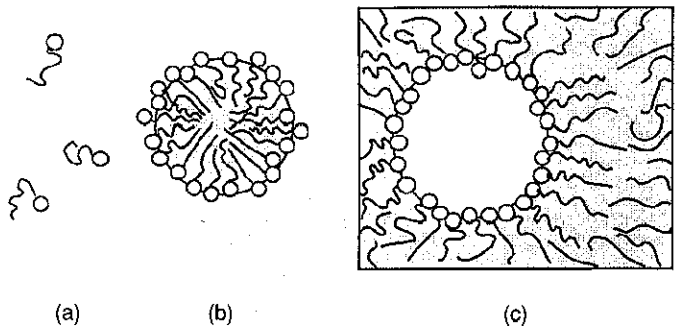

FIG. 2. Sample of phases that may be present in amphiphile/water systems: (a) conventional solution at very low amphiphile concentration, (b) micelle formation for concentrations above the critical micelle concentration (CMC), and (c) inverted micelles at high amphiphile concentrations. Other geometries are possible as well. In the diagram, the polar group of the molecule is indicated by a circle.

chain, the hydrophilic polar group at the head of the chain favors solvation. However, even at very modest concentrations of amphiphile, some fraction of the amphiphilic molecules undergo phase separation into *micelles,* as shown in Fig. 2. The abrupt onset of micelle formation occurs at the *critical micelle concentration* (or CMC). In an aqueous medium, the amphiphiles in a micelle are arranged so that their polar groups are in contact with water, while the nonpolar acyl chains aggregate in the interior of the micelle and are shielded from water. While micelle formation is favored energetically, it does not occur at very low amphiphile concentrations because of the low entropy of mixing compared to a conventional solution. Finally, at large amphiphile concentration, a phase of inverted micelles may form, also as indicated in Fig. 2.

The hydrocarbon chains of the micelle in Fig. 2(b) are packed together rather tightly, surrounded by the polar groups, which form a relatively close-packed array on the micelle surface to minimize the contact between the micelle interior and its aqueous environment. Thus, micelle formation is favored for amphiphiles whose polar head-group area is large compared to the transverse dimension of the hydrocarbon chains. In dual-chain lipids, the chains occupy proportionately more area than the head group does, and other phases, such as the lipid bilayers of Fig. 3, compete with micelle formation. Depending on the molecular geometry of the lipid, the most favored bilayer may be flat or curved. The ability of dual-chain lipids to form bilayers should not be interpreted as meaning that such lipids do not form micelles. In fact, because of the large hydrocarbon areas, the CMC of dual-chain lipids (typically 10^{-8} mol L^{-1}) is orders of magnitude smaller than that of single-chain lipids (typically 10^{-3} mol L^{-1}). Dual-chain lipids also are capable of forming phases of inverted micelles. As discussed further in Sec. 1.2, living cells are bounded by a plasma membrane whose structure includes a fluid lipid bilayer.

It is possible to obtain the elastic properties of biomembranes and related structures by several different techniques. An example of the micropipette aspiration technique is shown in Fig. 4, in which a cell or synthetic vesicle is drawn under pressure into a micropipette with a diameter of about a micron. Elastic moduli can be determined from the strain observed in the membrane when it is subject to a known stress. Another technique for measuring elastic moduli uses the fluctuations in cell geometry (see Sec. 2.4 for a de-

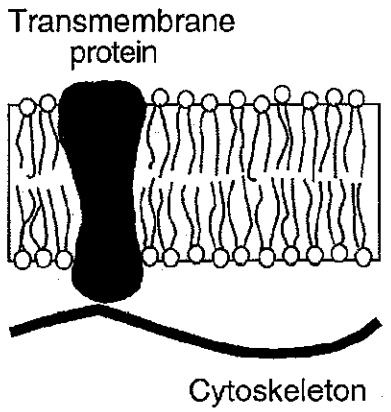

FIG. 3. Bilayer phase that may be present in amphiphile/water systems in which the amphiphile has two hydrocarbon chains. The bilayers in biomembranes are not chemically pure, and there may be proteins within the bilayer or attached to the bilayer as a cytoskeletal network.

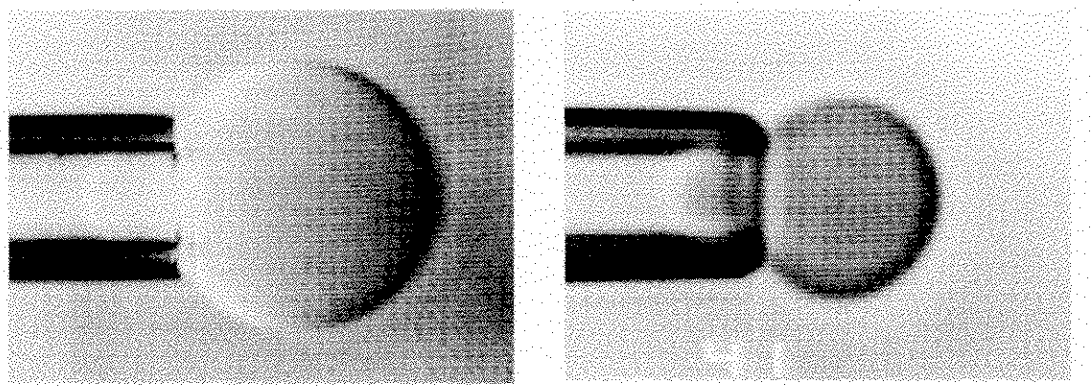

(a) (b)

FIG. 4. Micropipette aspiration of a giant phospholipid bilayer vesicle (left, diameter ~20 μm) and an osmotically preswollen red cell (right, diameter 6 μm). Several of the elastic constants of bilayers can be measured using variations of a technique in which the vesicle is subject to a known stress (from Mohandas and Evans, 1994).

scription of the bulk modulus in terms of volume fluctuations).

The bending moduli (k_b of Sec. 2.3) of phospholipid bilayers of biological importance typically are in the range (3–20) $\times 10^{-20}$ J, depending on chemical composition, and is in the same range as that reported for the red blood-cell plasma membrane using different techniques. While small compared to thin inorganic films, this modulus is about an order of magnitude larger than that of surfactant monolayers at an oil–water interface. The two-dimensional area compression modulus of a flat red-cell bilayer is 0.5 J/m^2, which may be more than an order of magnitude smaller than the product of the bilayer thickness and the volume compression modulus of a simple liquid such as water. Since bilayers are fluid, their shear modulus vanishes.

Depending on their geometry and other properties, lipids may form into bilayers that are flat or have a tendency to bend spontaneously (*spontaneous curvature;* see Sec. 2.3). A naturally curved bilayer may form into a closed geometry such as a sphere with no energy penalty. A spherical *vesicle* whose surface energy density depends only on the mean surface curvature has a relatively modest total energy of $8\pi k_b$ independent of the vesicle radius. This means that the deformation energy of the whole vesicle may be just (250–2000)k_BT for the range of moduli quoted above (where k_B is Boltzmann's constant and T is the absolute temperature). The size of the mesoscopic structures adopted by lipid bilayers covers a broad range: Stable vesicular systems that are found in Nature or that can be prepared in the laboratory vary from tens of nanometers to tens of microns.

Ternary mixtures of amphiphiles, oil, and water have very complicated phase diagrams, as one would expect. Micellar phases may be present, of course, and there are structures that can form with amphiphile at the interface between oil and water. Sponge phases also exist, in which oil and water are separated from each other in a labyrinth of three-dimensional channels running throughout the system. In this article, we concentrate on the self-assembled bilayers formed in binary systems.

1.2 Polymerized Membranes and Networks

The lipid bilayers described in Sec. 1.1 are fluid: they do not resist an in-plane shear. However, there are many inorganic monolayers or polymerized organic monolayers and bilayers that can support an in-plane shear (at least on small length scales, see Sec. 4.2). These materials are predicted to have different properties than fluid membranes, so we describe several examples here.

Graphite derives its lubricating properties from its molecular geometry consisting of

carbon rings linked together in a planar honeycomb structure. Other examples of planar inorganic monolayers can be obtained by a process known as exfoliation (Divigalpitiya *et al.*, 1989). This is a two-step process in which potentially reactive ions such as lithium are *intercalated* into layered structures such as MoS_2. In a second step, the intercalated material is exposed to water, which reacts strongly with the lithium and forces the monolayers apart. A section of an MoS_2 monolayer is illustrated in Fig. 5. Polymerized organic membranes can be obtained by exposing to ultraviolet radiation monolayers or bilayers of certain reactive organic compounds. The resulting materials are not always uniform, since polymerization may occur in local patches. A variety of materials have shown the ability to polymerize, many examples of which can be found in Ringsdorf (1988).

Two-dimensional networks also are examples of polymerized membranes. These networks need not be "solid" in the chemical sense—they only need to have a two-dimensional structure and fixed connectivity resulting in shear resistance. An example of a polymerized network is the spectrin cytoskeleton of the red blood cell (see Alberts *et al.*, 1989). The erythrocyte plasma membrane consists of three regions: the lipid bilayer forming the cell boundary, the glycocalix exterior to the cell, and the cytoskeleton on the interior or *cytoplasmic* side of the membrane. Tetramers of the spectrin protein (with a contour length of about 200 nm) form a two-dimensional network with largely triangular connectivity at the junction points of the spectrin tetrameres. The network is loose, with a mean separation between the junction complexes of 70 nm. A schematic representation of the cytoskeleton from a computer simulation is shown in Fig. 6, in which view (a) is perpendicular to the bilayer and view (b) is along the bilayer plane. The bilayer lies below the cytoskeleton in view (b). The in-plane shear modulus of this network, as measured by the micropipette experiments, is (6–9) $\times 10^{-6}$ J/m^2, although other experiments based on long-wavelength fluctuations have yielded lower values.

There is no reason to expect that all polymerized membranes or networks have uniform connectivity. For example, the erythrocyte cytoskeleton has approximately sixfold connectivity at its junction vertices, but the fraction of sixfold vertices is not 100%, and the connectivity of a given spectrin tetramer may not be fixed: There may be detachment and reattachment of spectrin, even if the rate is very slow. Further, there are hereditary

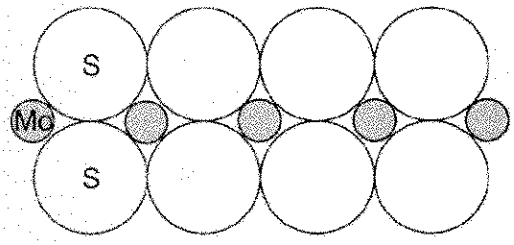

FIG. 5. Schematic drawing of a section through an MoS_2 monolayer. Such monolayers are formed by first intercalating the bulk material with reactive ions such as lithium, and then adding a solvent such as water that undergoes a reaction with the intercalant.

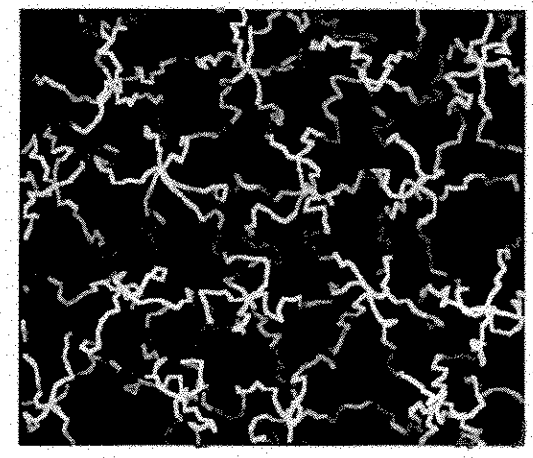

FIG. 6. Computer simulation of the membrane-associated cytoskeleton of the human erythrocyte. (a) The network seen from the cytoplasmic side of the membrane showing the sixfold connectivity of the cytoskeleton. (b) A section through the cytoskeleton. The lipid bilayer, not shown in (b), lies below the cytoskeleton.

diseases in which the spectrin concentration is depleted, resulting in incomplete networks and red cells with reduced elasticity (Mohandas and Evans, 1994).

1.3 Multilamellar Systems

One technique for vesicle production involves the swelling of multilayer (or *multilamellar*) stacks of dried lipid. Similar to, but much slower than, the production of inorganic monolayers by exfoliation described in Sec. 1.2, the invasion of water laterally through the stack forces the individual membranes apart. Not all bilayers in this procedure become separated from each other, and some remain in multilamellar structures. The bilayers in multilamellar systems are not always tightly bound to each other; there may be solvent trapped between lamellae, or several stacks of membranes may be linked by a single membrane. It is also possible to obtain more uniform multiple layers of material through the Langmuir–Blodgett technique (see Gaines, 1966). Small multilamellar stacks of membranes can be produced by the less gentle technique of applying high-frequency mechanical vibrations to lipid/solvent dispersions (sonication—see Fromherz *et al.*, 1986).

Part of the interest in multilamellar systems is the study of adhesion between bilayers. In some systems, thermal fluctuations of a membrane may prevent two membranes from adhering. These phenomena are treated in more detail in Sec. 6.

2. ELASTICITY

2.1 Deformations and the Strain Tensor

In one formulation of continuum mechanics, force is replaced by stress, and displacement is replaced by strain. Stress and strain can be represented by tensors, with the stress tensor having the dimensions of an energy density, while the strain tensor is dimensionless. In the statistical mechanics applications here, we use only the strain tensor; the reader interested in the more general formulation of continuum mechanics is referred to Fung (1994), Landau and Lifshitz (1986), or MECHANICAL PROPERTIES OF SOLIDS.

Consider the deformation of a two-dimensional square as shown in Fig. 7. Two-dimensional deformations are used here for diagrammatic simplicity; the notation is three dimensional. Two positions, marked by a and b on the undeformed square, define a vector $d\mathbf{x}$. A stress is applied to the square to change its shape and the points a and b move to new absolute positions, changing the vector $d\mathbf{x}$ to $d\mathbf{x}'$. Vectors $\mathbf{u}_a$ and $\mathbf{u}_b$ describe the displacement of positions a and b from the undeformed to the deformed state. The coordinate system does not change with the deformation.

Adding a constant displacement $\mathbf{u}$ to all positions on the object simply results in a translation of the object. In Fig. 7, the direction and magnitude of $\mathbf{u}$ vary locally, and the change of $\mathbf{u}$ with $\mathbf{x}$ provides a description of how vectors $\mathbf{x}$ at different locations on the object change with respect to each other. In our example, the vectors $d\mathbf{x}$ and $d\mathbf{x}'$ are related through

$$d\mathbf{x}' = d\mathbf{x} + \mathbf{u}_b - \mathbf{u}_a, \tag{1}$$

which can be written in the infinitesimal limit as

$$dx_i' = dx_i + \sum_j (\partial u_i/\partial x_j)dx_j, \tag{2}$$

where the components of each vector are indicated explicitly by the subscripts i and j.

The square of the length between neighboring points, dl^2, changes under the deformation to

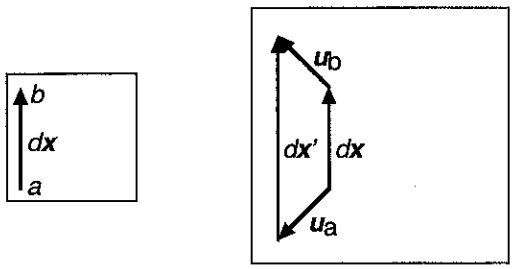

FIG. 7. Change in vector $d\mathbf{x}$ to $d\mathbf{x}'$ during a shape-preserving deformation. The initial object is shown on the left, while the deformed object is shown on the right. The initial position vector $d\mathbf{x}$ is superimposed on the deformed object to show the changes more clearly.

$$dl'^2 = dl^2 + 2\sum_{i,j} \epsilon_{ij} dx_i dx_j, \tag{3}$$

where

$$\epsilon_{ij} = \tfrac{1}{2}\left[\frac{\partial u_i}{\partial x_j} + \frac{\partial u_j}{\partial x_i} + \sum_k \frac{\partial u_k}{\partial x_i}\frac{\partial u_k}{\partial x_j}\right] \tag{4}$$

is the *strain tensor*. For deformations sufficiently small that terms quadratic in $\partial u_i/\partial x_k$ can be neglected, then the strain tensor can be approximated by

$$\epsilon_{ij} = \tfrac{1}{2}\left(\frac{\partial u_i}{\partial x_j} + \frac{\partial u_j}{\partial x_i}\right). \tag{5}$$

2.2 Elastic Moduli

Objects may deform in response to applied forces that, in general, may have complex orientations with respect to the object. For example, while an object may have a simple cubic shape, the forces on the object may be at oblique angles with respect to the surface of the cube. A spatial component of an applied force can be written in terms of the stress tensor σ_{ij} via $\Sigma_i \sigma_{ij} s_j$, where $\mathbf{s}$ is a vector whose magnitude is equal to the surface area to which the force is applied and whose direction is normal to the surface.

A spring is a simple example of a Hooke's-law object in which the strain (the displacement from equilibrium) is proportional to the stress (the applied force). Hooke's law can be generalized to the stress and strain tensors defined above, although the single spring constant must be replaced by more complex proportionality constants. One way of writing Hooke's law is

$$\sigma_{ij} = \sum_{p,q} c_{ijpq} \epsilon_{pq}, \tag{6}$$

where the constants c_{ijpq} are the elastic constants and have units of energy density. In principle, there are 36 elastic constants for three-dimensional materials, but if the elastic energy is a quadratic function of the strain, as it is in Hooke's law, then the maximum number of independent constants is 21. Further, the number of independent constants depends on the symmetry of the system, with isotropic systems having only two elastic constants.

We now consider an isotropic system in more detail. The change in free-energy density of deformation, ΔF, can be expanded in powers of the strain tensor, and the lowest-order terms in the expansion are quadratic in ϵ. Two independent scalar combinations of ϵ are available: the squared sum of the diagonal elements, $(\mathrm{tr}\epsilon)^2$, and the sum of the elements squared, $\Sigma_{i,j}\epsilon_{ij}^2$. If we assume that the deformations are small, then ΔF can be written as

$$\Delta F = (\lambda/2)(\mathrm{tr}\epsilon)^2 + \mu \sum_{i,j} \epsilon_{ij}^2. \tag{7}$$

The constants λ and μ are called the Lamé coefficients, of which μ is the shear modulus. The compression modulus K can be expressed in terms of the Lamé coefficients by

$$K_A = \lambda + \mu \quad \text{(two dimensions)}, \tag{8a}$$

$$K_V = \lambda + 2\mu/3 \quad \text{(three dimensions)}. \tag{8b}$$

Both K and μ must be positive, or else the system could spontaneously deform by a shear or compression mode. The Lamé coefficient λ is not constrained to be positive, and systems are known in which λ is negative.

A further quantity of interest is the Poisson ratio σ_{P}, which is a measure of how much a material *contracts* in the transverse direction when it is stretched in the longitudinal direction. The geometrical definition of σ_{P} is then $-\epsilon_{yy}/\epsilon_{xx}$ for a deformation u_x in the x direction that results in a displacement u_y in the y direction. Poisson's ratio can be expressed in terms of elastic constants by

$$\sigma_{\mathrm{P}} = (K_A - \mu)/(K_A + \mu) \quad \text{(two dimensions)}, \tag{9a}$$

$$\sigma_{\mathrm{P}} = (3K_V - 2\mu)/(6K_V + 2\mu) \quad \text{(three dimensions)}. \tag{9b}$$

As an application, we consider a triangular network of springs in two dimensions, as shown in Fig. 8. The elastic moduli can be found by evaluating the energy change of a specific deformation and comparing the result with Eq. (7). At zero temperature, one finds

$$K_A = \sqrt{3}k_{sp}/2 \tag{10}$$

and

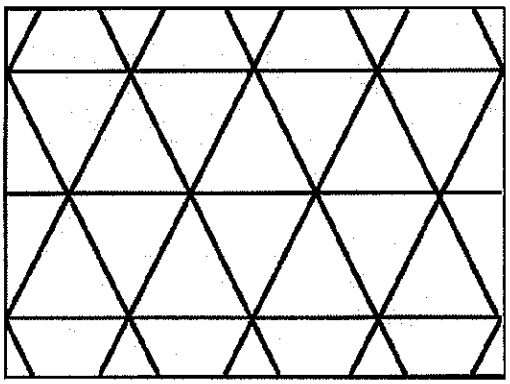

FIG. 8. Triangular network of springs in two dimensions.

$$\mu = \sqrt{3}k_{sp}/4 = K_A/2, \tag{11}$$

where k_{sp} is the spring constant. Note that both moduli are independent of the unstretched spring length. The Poisson ratio for this network is then

$$\sigma_P = \tfrac{1}{3}. \tag{12}$$

This sign of the Poisson ratio indicates that when the network is stretched in one direction, it contracts in the transverse direction. Many solids have a Poisson ratio of about $\frac{1}{3}$ in three dimensions. Some networks under tension are predicted to have a negative Poisson ratio.

2.3 Bending Resistance

The compression modulus is a measure of the free-energy change when the elements of a structure are forced closer together under pressure, or pulled further apart under tension. When the membranes illustrated in Figs. 3 and 5 are forced to bend, say about an axis pointing out of the plane of the diagram, then elements on one side of the midplane are forced closer together, while elements on the other side move farther apart. The free-energy change associated with the bending deformation is a measure of the bending resistance.

Just as with the shear and compression deformations of Secs. 2.1 and 2.2, we first need to develop a geometrical description of the bending of a surface. Following the approach of Safran (1994), we begin by reviewing the description of a curved line. In a coordinate system external to the line, each point on the curve is specified by a vector **R**, as in Fig. 9. The distance in space dl between two points separated by an infinitesimal arc length ds is then

$$dl = \left|\frac{\partial \mathbf{R}(s)}{\partial s}\right| ds, \tag{13}$$

where $|\mathbf{R}|$ represents the length of vector **R**. The unit vector normal to the curve, **n**, is proportional to the second derivative of the position vector:

$$C\mathbf{n}(s) = \frac{d^2\mathbf{R}(s)}{dl^2}, \tag{14}$$

where C is the curvature.

Now, the above description must be generalized for a two-dimensional surface embedded in three dimensions. Consider the surface shown in Fig. 10. Each point on the surface is specified by a height $h(x,y)$, which is a function of the fixed coordinate system x and y. In the figure, there is only one surface element for each (x,y) pair—there are no overhangs, and $h(x,y)$ is single-valued. We assume that the membrane of interest is sufficiently flat that this representation, referred to as the Monge representation, is valid.

The figure also shows vectors **n** normal to the surface. At each point (x,y), the normal has coordinates

$$\mathbf{n}(x,y) = (-\partial_x h, -\partial_y h, 1)/(1 + |\nabla h|^2)^{1/2}, \tag{15}$$

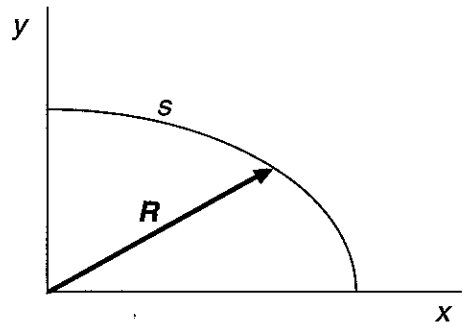

FIG. 9. Coordinates of a curve. The arc length s is the coordinate along the curve, while **R** is the position of a particular point on the curve, as measured with respect to an external coordinate system.

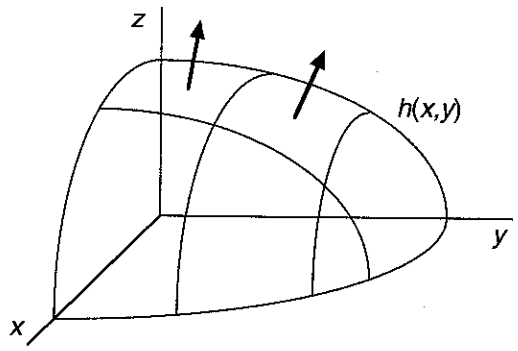

FIG. 10. Coordinates of a surface. Each element on the surface is described by its height $h(x,y)$ above the xy plane. Normals to the surface are indicated by bold arrows.

where ∂_x is $\partial/\partial x$. While there is a unique curvature associated with a given point on a line in Eq. (14), the curvature on a surface has a direction dependence that reflects the orientation of the vector $d\mathbf{R}$ along the surface:

$$C = -(d\mathbf{R}\cdot d\mathbf{n})/(d\mathbf{R}\cdot d\mathbf{R}). \tag{16}$$

Clearly, one has to establish a set of directions along which to evaluate the curvature, and the method of choice is to construct a curvature tensor $\mathbf{C}$ such that

$$d\mathbf{n} = d\mathbf{R}\cdot\mathbf{C}. \tag{17}$$

The eigenvalues of $\mathbf{C}$ are referred to as the principal curvatures, which we denote by C_1 and C_2. Note that there is no requirement that C_1 and C_2 have the same sign: a saddle point, for example, has principal curvatures of opposite sign.

The curvature tensor provides the geometrical description of a bending deformation, much as the strain tensor describes compression and shear in Sec. 2.1. Further, the free energy can be written as a function of the principal curvatures, as is done for the strain tensor in Sec. 2.2. The curvatures are usually written in the combinations $(C_1 + C_2)/2$ and C_1C_2, which are the mean curvature and Gaussian curvature, respectively. Expressed in terms of the principal curvatures, the leading-order terms in the free-energy density for bending, F, are

$$F = (k_b/2)(C_1 + C_2 - 2C_0)^2 + k_gC_1C_2, \tag{18}$$

where k_b is the bending rigidity and k_g is the Gaussian rigidity. The addition of the parameter C_0, referred to as the spontaneous curvature, allows for situations in which the membrane intrinsically bends to one side. The Gaussian rigidity is often omitted from expressions for the free energy in situations where the topology of the surface is closed, since the integral of the Gaussian curvature over a closed surface is a topology-dependent constant. The shapes of closed surfaces subject to bending resistance, as in Eq. (18), are discussed in VESICLES AND BIOMEMBRANES.

2.4 Elasticity and Fluctuations

The elastic moduli are introduced in Sec. 2.2 as terms in an expansion of the free-energy density. This approach is useful in statistical mechanics problems, since the weight accorded to a specific configuration in an ensemble is $\exp(-\beta E)$, where E is the energy of the configuration and β is the inverse temperature $(k_BT)^{-1}$. Statistical mechanics provides a description of the elastic moduli based on ensemble averages.

Consider the isothermal compression modulus, K_V, as an example. The physical definition of K_V is

$$K_V = -\frac{V}{\partial V/\partial P}, \tag{19}$$

where V is the volume of the system and P is the applied pressure. In an alternative approach that emphasizes the fluctuations in the system at nonzero temperature, the Gibbs free energy is expanded about the equilibrium value at a fixed pressure (Reif, 1965):

$$\Delta G = G(V) - G(V_{eq}) = (V - V_{eq})^2/(2V_{eq}K_V), \tag{20}$$

where V_{eq} is the equilibrium value of the volume. The corresponding partition function can be evaluated analytically, since the weight for a given volume V is proportional to $\exp(-\beta\Delta G)$. As a result, the compression modulus also can be expressed as

$$\beta K_V = \langle V\rangle/(\langle V^2\rangle - \langle V\rangle^2), \tag{21}$$

where $\langle V\rangle$ is the ensemble average of V.

A formally identical problem to this is the relation between the fluctuations in the length of a spring and the spring constant k_{sp}. The expression analogous to Eq. (21) is

$$\beta k_{sp} = (\langle l^2 \rangle - \langle l \rangle^2)^{-1}, \tag{22}$$

where l is the length of the spring. Note that Eq. (22) is independent of the unstretched spring length.

3. FLEXIBLE CHAINS

3.1 Ideal Chains

Linear and branched chains provide an intuitive introduction to the geometrical and elastic properties of membranes. We pause to assemble a number of results from polymer physics that will put the behavior of membranes in context.

The simplest geometry of a single polymer chain is one in which a chain element, or monomer, is freely jointed and can assume any orientation irrespective of the orientation of its neighbors. The conformations of the chain are equivalent to a random walk if the chain elements are permitted to intersect each other. Consider the situation in which the elements of the chain are represented by vectors $\mathbf{a}_i$, each of which has the same length a. A chain with N segments has a contour length along the chain of Na. Of interest is the end-to-end displacement vector $\mathbf{r}_{ee}$, illustrated in Fig. 11, which is just the sum of the individual vectors: $\mathbf{r}_{ee} = \Sigma_i \mathbf{a}_i$. The ensemble average over all possible conformations at fixed N yields the well-known result

$$\langle r_{ee}^2 \rangle = Na^2. \tag{23}$$

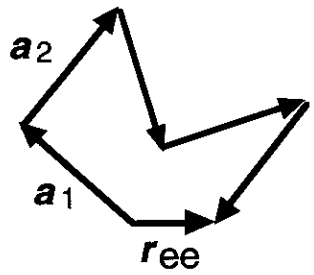

FIG. 11. End-to-end displacement $\mathbf{r}_{ee}$ for a chain whose elements have a common length and random orientation.

Thus, the end-to-end displacement grows with contour length like $N^{1/2}$. Other geometrical quantities, such as the radius of gyration, also scale like $N^{1/2}$.

Consider now the slightly more complicated problem of chains with a fixed polar angle θ between successive segments i and $i + 1$, such that

$$\mathbf{a}_i \cdot \mathbf{a}_{i+1} = -a^2 \cos\theta, \tag{24}$$

where the convention is that $\theta = 0$ if neighboring segment vectors $\mathbf{a}_i$ point in opposite directions. Although the polar angle between segments is fixed, the azimuthal angle is not, and the segments are free to rotate around one another. As shown in Flory (1953), the end-to-end displacement of this chain at large N is

$$\langle r_{ee}^2 \rangle = Na^2(1 - \cos\theta)/(1 + \cos\theta). \tag{25}$$

The important feature to note in Eq. (25) is that the end-to-end displacement scales like $N^{1/2}$, in spite of the restrictions on the chain's conformations. In fact, the $N^{1/2}$ scaling is found for all chains on sufficiently large length scales, so long as the chain path can cross itself. It is then useful to introduce the idea of an effective bond length b which reflects the length scale at which the chains appear to be ideal; that is, $\langle r_{ee}^2 \rangle = Nb^2$. The effective bond length has the same order of magnitude as the persistence length, which measures the length scale over which the spatial orientation of the monomers is correlated [see Eq. (43)]. For the restricted orientation situation of Eq. (25), the effective bond length is

$$b = a[(1 - \cos\theta)/(1 + \cos\theta)]^{1/2}. \tag{26}$$

In alkane chains (the hydrocarbon chains present in soap, for example), θ is close to the tetrahedral angle of 109.5°, and the effective bond length is $\sqrt{2}a$, according to Eq. (26), or about 0.2 nm. Their rigidity and monomer size dictate that protein chains have considerably longer effective bond lengths, several nanometers or more, depending on the protein. Of course, steric interactions prevent physical systems, such as proteins, from intersecting themselves, and so their behavior is not described fully by ideal-chain scaling.

3.2 Self-Avoiding Chains

While the "ideal chains" of Sec. 3.1 may intersect themselves, physical systems have

an excluded volume that enforces self-avoidance of the chain. This steric interaction among the chain elements is important for chains in one-, two-, and three-dimensional systems. Consider the simple situation in which a chain lies along the x axis. Self-avoidance forbids the chain from reversing on itself from one step to the next, so that the end-to-end distance must be just the contour length Na. But Eq. (23) shows that $\langle r_{ee} \rangle$ scales like $N^{1/2}$ for ideal chains, *independent of embedding dimension.* Thus, we conclude that in one dimension, self-avoidance of the chain dramatically affects its scaling properties. The same conclusion can be drawn for chains in two and three dimensions.

A simple model for the length-scaling exponent of self-avoiding chains was proposed by Flory (1953). The calculation evaluates the power-law dependence of the free energy on the effective chain size r and number of segments N at both large and small r. Minimizing the free energy yields r as a function of N. Since our goal is to extract the scaling exponent, we do not pay close attention to numerical factors like $4\pi/3$, and we use r to represent the effective size of the chain, as characterized by an end-to-end length or a root mean square radius. Also, our model chains have no explicit energy scale other than the temperature. Following de Gennes (1979), the behavior of the free energy is evaluated in two regimes:

1. Short distances. Steric repulsion between the chain segments causes the chain to swell compared to an ideal chain. The repulsive energy experienced by one segment through its interaction with other segments is proportional to the concentration of segments, roughly N/r^d for a chain in a d-dimensional space. Thus, the total repulsive energy experienced by all N segments is proportional to N^2/r^d. Now, the repulsive energy also will be proportional to the excluded volume of the segment–segment interaction, which we characterize by a parameter v_{ex}. Taking the excluded volume as a hard-core interaction, then the energy scale of the interaction is set by the temperature k_BT. Thus, the steric contribution to the free energy should behave like

$$F = k_B T v_{ex} N^2 / r^d, \tag{27}$$

where all constants have been absorbed into v_{ex}.

2. Long distances. As a chain is stretched, the number of configurations that it can adopt at a fixed end-to-end distance decreases rapidly. As shown in Sec. 3.4, the probability of finding a given end-to-end distance r for an ideal chain decays exponentially as $\exp(-dr^2/2Na^2)$, where a is the elementary segment length. Recalling that the entropy S is proportional to the logarithm of the probability, then to within a constant

$$S/k_B = -dr^2/2Na^2. \tag{28}$$

The entropic contribution to the free energy at long distances can be found through $F = E - TS$. Combining Eqs. (27) and (28) and discarding overall normalization constants, the free energy of the self-avoiding chain behaves like

$$F = k_B T v_{ex} N^2 / r^d + k_B T d r^2 / 2Na^2. \tag{29}$$

This expression shows that there is a penalty for pushing the chain elements close together (small r), and there is a penalty for stretching out the chains (large r). The value for r that minimizes F can be found by taking the derivative of Eq. (29) with respect to r, holding other quantities fixed, and this value scales like

$$r \approx N^{3/(2+d)}. \tag{30}$$

The scaling behavior of Eq. (30) is expected for any length scale r that characterizes the linear dimension of the system as a whole, such as the end-to-end distance r_{ee} and the root mean square radius of the system $(\langle r_{ee}^2 \rangle^{1/2}/\sqrt{6})$. The exponent on the right-hand side of Eq. (30) is called the Flory exponent.

The systems discussed thus far in this section are linear chains. Chains with side branches, referred to as branched polymers, have different scaling with system mass N than do linear chains, since branching will add monomers to a given position along the chain. Because a branched polymer has more than two ends, the end-to-end displacement is replaced as a measure of the polymer size by some other quantity such as the radius of gyration R_g, defined by

$$R_g^2 = \sum_i (\mathbf{r}_i - \mathbf{r}_{\text{c.m.}})^2, \tag{31}$$

where $\mathbf{r}_{\text{c.m.}}$ is the center-of-mass position of the chain and the sum is over the positions of the segments. The radius of gyration for branched polymers is found to have a scaling form

$$\langle R_g^2 \rangle \approx N^{2\eta}. \tag{32}$$

The branched-polymer scaling exponents are smaller than the self-avoiding walk exponents, being 0.64 and 0.5 in two and three dimensions respectively, compared to 0.75 and 0.59 for self-avoiding walks. The scaling exponents for linear and branched polymers are summarized in Table 1.

In real polymers, the chains may be rigid because of bond-angle restrictions, and there may be attractive van der Waals interactions between monomers. What effects do these interactions have on scaling behavior? As shown in Sec. 3.1, making chains stiffer only increases the persistence length of the chain; it does not change the scaling behavior in the large-N limit. Of course, for small N the introduction of rigidity may change the appearance of the chain configuration substantially. The situation is different if there is attraction between chain elements. If the attraction is strong enough, then the chains collapse to a dense phase in which the chain size scales like $N^{1/d}$. For example, self-avoiding walks in three dimensions without attractive interactions scale like $N^{3/5}$, but for strong attraction they scale like $N^{1/3}$. The transition between the two scaling regimes is a phase transition and occurs at a temperature (or attraction strength) called the Θ point.

3.3 Self-Avoiding Rings

Let us close our linear chain to form a loop in two dimensions, which will serve as a two-dimensional vesicle. Closing the chain introduces a new characteristic, namely, the enclosed ring area, as well as the conjugate thermodynamic variable of pressure P. The parameter space of the rings then includes bending rigidity, van der Waals attraction, and pressure.

We consider the effects of each parameter in turn, with the others set equal to zero.

1. Rigidity. The presence of rigidity changes the persistence length, but not the asymptotic scaling behavior at large N, although the scaling behavior at finite N is nontrivial.
2. Pressure. Defining

$$\Delta P = P_{\text{inside}} - P_{\text{outside}}, \tag{33}$$

then at $\Delta P > 0$, the ring is always inflated at large N and the scaling behavior is $\langle R_g^2 \rangle \approx N^2$ and $\langle A \rangle \approx N^2$. At zero pressure, the ring should behave like a self-avoiding walk, with $\langle R_g^2 \rangle \approx N^{3/2}$ and $\langle A \rangle \approx N^{3/2}$. When the outside pressure exceeds the inside pressure ($\Delta P < 0$), the ring belongs to the branched polymer family but is not dense. For the ring to look like a branched polymer, it must have little enclosed area, so that $\langle R_g^2 \rangle \approx N^{1.28}$ and $\langle A \rangle \approx N$.
3. Attraction. If the attraction between monomers on the chain is strong enough, then the configurations may become dense, and $\langle R_g^2 \rangle \approx N$ and $\langle A \rangle \approx N$. This is similar to the Θ point of linear polymers.

A summary of the scaling exponents is given in Fig. 12 for two-dimensional rings simultaneously subject to pressure and attraction (Boal, 1991).

Table 1. Scaling exponents η for the scaling law $\langle R_g^2 \rangle \sim N^{2\eta}$ for ideal or random walks, self-avoiding walks, and branched polymers as a function of embedding dimension d.

Configuration	$d = 2$	$d = 3$
Random walk	1/2	1/2
Self-avoiding walk	3/4	0.59
Branched polymer	0.64	1/2

3.4 Chain Elasticity

There are comparatively few configurations in which an ideal chain is fully stretched: The most common configurations are ones in which the chain is highly convoluted. Since entropy is proportional to the logarithm of the number of configurations, then another way of stating this observation is that the entropy of the chain is reduced, and the free energy is increased, as a chain is stretched. This implies that the chain has elasticity arising from its entropy.

To find the relationship between the elas-

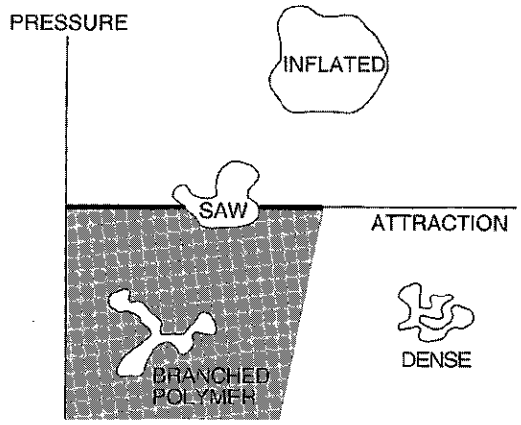

FIG. 12. Phase diagram for two-dimensional self-avoiding rings subject to pressure and attraction. There may be considerable finite-size scaling effects near the phase boundaries.

ticity of an ideal chain and its geometry, we consider the distribution of end-to-end vectors $\mathbf{r}_{ee}$. Let us break up the three-dimensional distribution into three one-dimensional distributions. The x component of the end-to-end displacement, $r_{ee,x}$, is just the sum of the individual monomer segment lengths projected onto the x axis: $r_{ee,x} = \Sigma_i a_{i,x}$. For ideal chains, $a_{i,x}$ is uncorrelated with $a_{i+1,x}$, and the situation is the same as the one-dimensional random walk with steps of variable size. In the continuum limit, the probability of finding a one-dimensional walk with end-to-end displacement between x and $x + dx$ is just

$$\rho(x)dx = (2\pi Na^2/d)^{-1/2} \exp(-dx^2/2Na^2)dx, \tag{34}$$

where $\rho(x)$ is the probability density (probability per unit length) and d is the embedding dimension. This distribution is normalized to unity and has expectations

$$\langle r_{ee,x} \rangle = \int x\rho(x)dx = 0 \tag{35}$$

and

$$\langle r_{ee,x}^2 \rangle = \int x^2\rho(x)dx = Na^2/3 \tag{36}$$

for the x component of the end-to-end displacement vector in three dimensions.

Equations (35) and (36) can be used with Eq. (22), which relates the spring constant to the fluctuations in spring length, to obtain an expression for the effective spring constant of the chain:

$$k_{sp} = dk_B T/Na^2. \tag{37}$$

Equation (37) shows that the effective stiffness of the chain increases with d and the temperature T. The elastic behavior of the chain is entropic in origin, since there is no potential-based restoring force at the microscopic level.

4. FLUCTUATING MEMBRANES

4.1 Fluid Membranes

The lipid bilayer component of a cell's plasma membrane is a fluid in the sense that it cannot resist an in-plane shear. In the absence of bending rigidity or in-plane shear resistance, fluid membranes can assume convoluted shapes and are, in a sense, the two-dimensional analogs of freely jointed chains. The geometry of membranes can be described using similar scaling relationships to those used to describe linear and branched chains (see Secs. 3.1–3.3).

Closed configurations, such as spherical or toroidal geometries, have a larger number of scaling observables than do open configurations. An example of a closed fluid membrane with the topology of a sphere is shown in Fig. 13. If the membrane had a sufficiently large value for k_b, then the spherical shape would be obvious, but in fact, the membrane shown in Fig. 13 has $k_b = 0$. The shape is reminiscent of a branched polymer, in that the enclosed volume is proportional to the area, rather than the area to the $\frac{3}{2}$ power expected for a sphere. An analysis performed via computer simulation confirms that closed fluid membranes obey the same branched polymer scaling as self-avoiding surfaces (Kroll and Gompper, 1992):

$$\langle R_g^2 \rangle \sim A^1, \tag{38a}$$

$$\langle V \rangle \sim A^1. \tag{38b}$$

The generalized Flory exponent [see Eq. (30)] for self-avoiding surfaces is

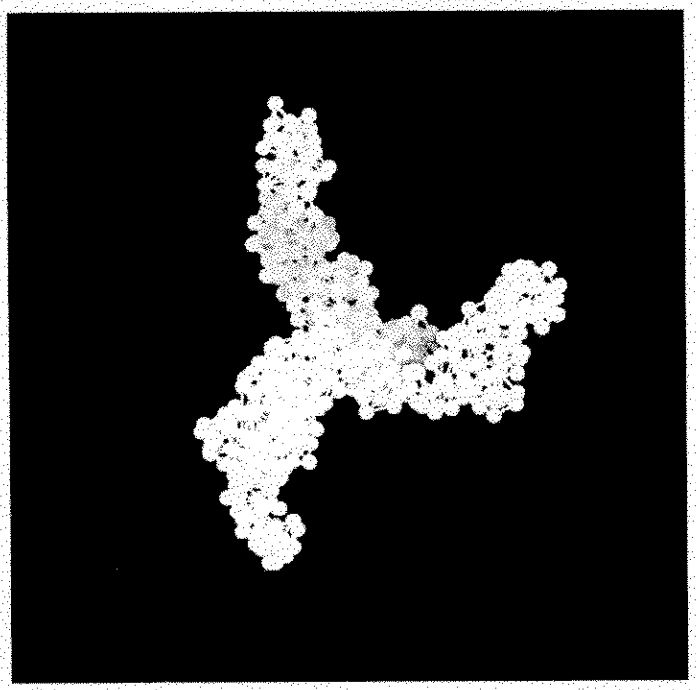

FIG. 13. Sample configuration from a computer simulation of a fluid membrane with spherical topology. The surface, which has no bending resistance, is represented by discrete points: hard beads linked together by tethers of a maximal extension. The beads are not attached to a fixed set of neighbors, but can migrate through the membrane.

$$\nu_F = (2 + D)/(2 + d), \tag{39}$$

where D is the dimension of the surface ($D = 1$ for chains, $D = 2$ for membranes) and d is the embedding dimension (see lectures by Kantor in Nelson *et al.*, 1989). Equation (39) predicts that $\langle R_g^2 \rangle \sim A^{0.8}$ for a fluid membrane in three dimensions, but this scaling behavior has been seen only for moderate system sizes, not large systems. Fluid membranes with bending resistance also belong to the class of branched polymers, although the distance at which the asymptotic scaling behavior becomes apparent increases with k_b. Again, this is like the scaling of chains with bending resistance described in Sec. 3.1.

Fluid-membrane undulations, at distances short compared to the persistence length, can be treated using the Monge representation (see Sec. 2.3). The mean square fluctuation in the height $h(\mathbf{r})$ at position $\mathbf{r}$ is predicted to vary as

$$\langle h(\mathbf{r})^2 \rangle \sim TL^2/k_b, \tag{40}$$

where T is the temperature and L is the linear dimension of the system (see Safran, 1994). This relationship demonstrates that the fluctuations increase with temperature and system size. In contrast, the mean square undulations at an interface dominated by surface tension (between water and air, for example) grow only logarithmically with the system dimension L.

The membrane height can be expressed in terms of its Fourier components $h_{\mathbf{q}}$ via

$$\langle h(\mathbf{r})^2 \rangle = A^{-1} \sum_{\mathbf{q}} \langle |h_{\mathbf{q}}|^2 \rangle \tag{41}$$

where A is the membrane area. The Fourier components corresponding to Eq. (40) scale as

$$\langle |h_{\mathbf{q}}|^2 \rangle \sim T/k_b q^4. \tag{42}$$

In comparison, the Fourier components of the height of an interface dominated by surface tension scale like $\langle |h_{\mathbf{q}}|^2 \rangle \sim T/q^2$. Experimental observations of membranes under tension are consistent with the undulation spectrum of Eq. (42) (see references in Mohandas and Evans, 1994).

Because of surface undulations, the normals to the surface $\mathbf{n}(\mathbf{r})$ are correlated only at short distances. That is, the product of two normals decays with displacement $\mathbf{r}$ as

$$\langle \mathbf{n}(0) \cdot \mathbf{n}(\mathbf{r}) \rangle \sim \exp(-|\mathbf{r}|/\xi_p), \tag{43}$$

where ξ_p is the persistence length. Perturbation theory can be used to calculate the low-temperature fluctuations of a membrane whose energy is characterized by a bending modulus k_b, as in Eq. (18), yielding a persistence length of (see lectures by Leibler in Nelson *et al.*, 1989)

$$\xi_p \sim a \exp(4\pi\beta k_b/3), \tag{44}$$

where a is a microscopic length scale and β is the inverse temperature $(k_B T)^{-1}$. The numerical factors in the exponential depend on the method used for the calculation. What is important about Eq. (44) is that the persistence length is exponential in the bending rigidity.

The persistence length of a chain sets the length scale above which bending resistance and other geometrical constraints are sufficiently unimportant that the chain conformations are described by a random walk. Another way of saying this is that the effective bending resistance of the chain decreases with the increasing length scale on which the resistance is measured. The behavior of fluid sheets can be viewed in the same way, that the effective bending modulus $k_{b,\text{eff}}$ decreases with the increasing length scale of the system. Again, perturbation theory consistent with Eq. (44) indicates that to leading order, the effective bending resistance has the form

$$k_{b,\text{eff}}(L) = k_b[1 - (3/4\pi\beta k_b) \ln(L/a)], \tag{45}$$

where L is the length scale of interest (see lectures by Leibler in Nelson *et al.*, 1989).

4.2 Polymerized Membranes

Polymerized membranes and networks have fixed connectivity, by which we mean that a given element of the membrane has a fixed set of neighbors, as distinct from fluid membranes in which an element can diffuse through the membrane. The shear rigidity imparted by fixed connectivity results in constraints on the configuration space of the membrane, which, in turn, affect its scaling behavior. The shape of the fluid membrane in Fig. 13 easily can be seen to be different from the shape of the polymerized membrane in Fig. 14: The fluid membrane is convoluted whereas the polymerized membrane is flat.

Scaling analyses of open polymerized membranes show that

$$\langle R_g^2 \rangle \sim A^1, \tag{46a}$$

$$\langle h^2 \rangle \sim A^\zeta, \tag{46b}$$

where A is the contour area (or mass) of the membrane and ζ is the roughness exponent. The mean square height $\langle h^2 \rangle$ in Eq. (46b) measures the thickness of the membrane and is the smallest eigenvalue of the membrane's inertia tensor. First measured to be 0.65 ± 0.05 (Plischke and Boal, 1988), the roughness exponent obtained from recent computer simulations is close to the field-theoretic prediction of 0.59 (Le Doussal and Radzihovsky, 1992).

The polymerized membrane in Fig. 14 is flat in spite of the fact that it has no local bending resistance: $k_b = 0$. The membrane becomes increasingly rigid at long length scales because of geometrical constraints im-

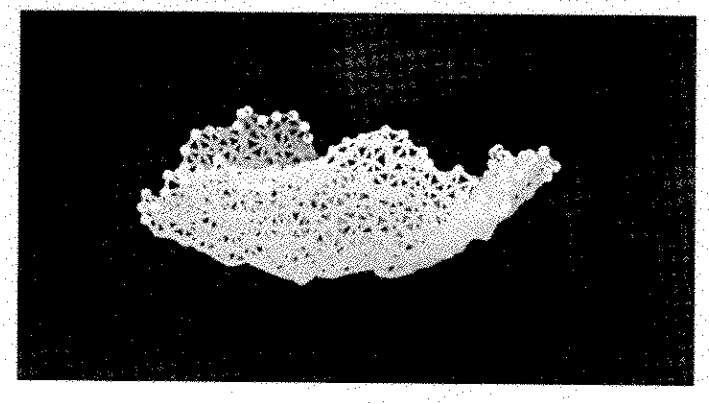

FIG. 14. Sample configuration from a computer simulation of an open polymerized membrane with no local bending resistance. As in Fig. 13, the surface is represented by discrete points; but here, the beads are attached to a fixed set of neighbors.

posed by polymerization. As experimentation with aluminum foil will convince the reader, an initially flat polymerized membrane cannot even approximate the configuration shown for the fluid membrane in Fig. 13 without extensive folding of the surface, and such folding is strongly suppressed by entropy. Thus, the effective bending resistance $k_{b,\text{eff}}$ of a polymerized membrane should increase with length scale L, rather than decrease as found for fluid membranes. Several calculations show that $k_{b,\text{eff}}$ diverges like $L^{2-2\zeta} \sim L^{0.8}$ (see Nelson *et al.*, 1989).

Although the bending resistance of a polymerized membrane increases with L, other in-plane moduli are expected to decrease with L because of undulations. Calculations of the in-plane area compression modulus and shear modulus both show moduli that vanish at large L, as, for example,

$$\mu \sim L^{-(4\zeta-2)} \sim L^{-0.4}. \tag{47}$$

Most of these predictions have been confirmed by computer simulation. Further, the Poisson ratio of polymerized networks is predicted to be universally equal to $-\frac{1}{3}$ (Le Doussal and Radzihovsky, 1992).

Experimental tests of the analytic and simulation results thus far have addressed whether polymerized membranes are flat, and not all of the measurements are in agreement. One set of measurements on the isolated two-dimensional cytoskeleton of the red blood cell indicates that the network is flat on long length scales. Other work on inorganic monolayers does not support this finding.

4.3 Membranes under Stress

The membranes discussed in Secs. 4.1 and 4.2 are isolated, in the sense that they are not subject to external stress nor do they interact with a medium or with other membranes. However, a complete description of physical membrane behavior must include the characteristics of interacting membranes. In this section, the effects of compression and tension on membranes will be described, while interactions between membranes are presented in Sec. 6.

4.3.1 Closed Fluid Membranes Closed fluid membranes with spherical topology (a computational *vesicle*) subject to pressure have been simulated both for surfaces whose elements are plaquettes on a lattice and for triangulated surfaces that are not constrained to lie on a lattice, and whose connectivity can evolve with time (as in Fig. 13). Both rings in two dimensions (Sec. 3.3) and fluid vesicles in three dimensions obey branched-polymer scaling under compression, but only vesicles show branched-polymer scaling at zero pressure. Depending on the vesicle mass, the scaling may remain branched-polymer even if the pressure inside the vesicle moderately exceeds the pressure outside; however, at large pressure differences, there is a transition to an inflated state.

4.3.2 Open Membranes at a Wall The interaction between a membrane and a wall has been investigated for two situations: a sheet forced against a flat surface by pressure and a sheet confined between two flat surfaces. The presence of the wall removes the divergence in the fluctuation spectrum of fluid membranes observed at long wavelengths [Eq. (42), see Safran, 1994]. The behavior of polymerized membranes near walls can be used to determine the roughness exponent.

4.3.3 Planar Membranes under Tension Observed at sufficiently short length scales, membranes under tension, or membranes with bending resistance, are relatively flat. The elasticity of a planar, polymerized network of springs under tension has been investigated by simulation. At zero temperature, the in-plane elastic moduli vary with stress σ as

$$K_A/k_{sp} = (3^{1/2}/2)(1 - \sigma/3^{1/2}k_{sp}), \tag{48a}$$

$$\mu/k_{sp} = (3^{1/2}/4)(1 + 3^{1/2}\sigma/k_{sp}), \tag{48b}$$

where positive σ corresponds to a network under tension and k_{sp} is the spring constant of an individual spring. These expressions, which have Eqs. (10) and (11) as their zero-stress limit, predict that the Poisson ratio of the network becomes negative when $\sigma/k_{sp} > \sqrt{3}/5$. At finite temperature, in-plane fluctuations increase the moduli above their zero-temperature values.

5. SYSTEMS WITH DEFECTS

5.1 Percolation Phenomena

The networks and membranes typically found in Nature are not the ideal, uniform systems that are considered in Sec. 4. Rather, they may be chemically inhomogeneous and/or may contain structural defects. Two examples of defective membranes and networks are mentioned in Sec. 1.2: partially polymerized membranes in which polymerization is random or localized, and spectrin-depleted erythrocyte cytoskeleta in which the coordination of some junction complexes may be much less than sixfold. Further, defects may develop in otherwise regular membranes and networks when they are subject to stress or elevated temperatures, leading ultimately to mechanical failure. These structural aspects of membranes are an active area of study in statistical mechanics, although the investigation of systems with defects dates back more than a century to Maxwell.

One very useful concept that emerged from computational studies of defective systems is that of *percolation*. Consider the two-dimensional triangulated network shown in Fig. 15, in which the light gray "bonds" are fluid (as in Fig. 13), while the white "bonds" are polymerized and connected to a fixed set of vertices (as in Fig. 14). If most or all of the bonds are fluid, then the shear modulus of the network vanishes. There must be a reasonable concentration of polymerized bonds present before the network exhibits shear resistance. Computer simulations of systems such as this have shown that

1. there is a well-defined concentration, referred to as the *rigidity percolation* threshold p_r, above which networks resist shear; and
2. there is a well-defined concentration, referred to as the *connectivity percolation* threshold p_c, above which a connected sequence of polymerized bonds completely traverses the network,

where p may be defined as the fraction of polymerized bonds present in the network compared to the fully polymerized network, for which $p = 1$. In Fig. 15, p is greater than p_c, and uninterrupted paths of polymerized bonds can be seen in both the x and y directions. There are many examples in which the connectivity and rigidity thresholds are different (Thorpe, 1986).

5.2 Defective Two-Dimensional Networks

Connectivity and rigidity percolation occur at the same polymerized bond concentration in the mixed-composition network of

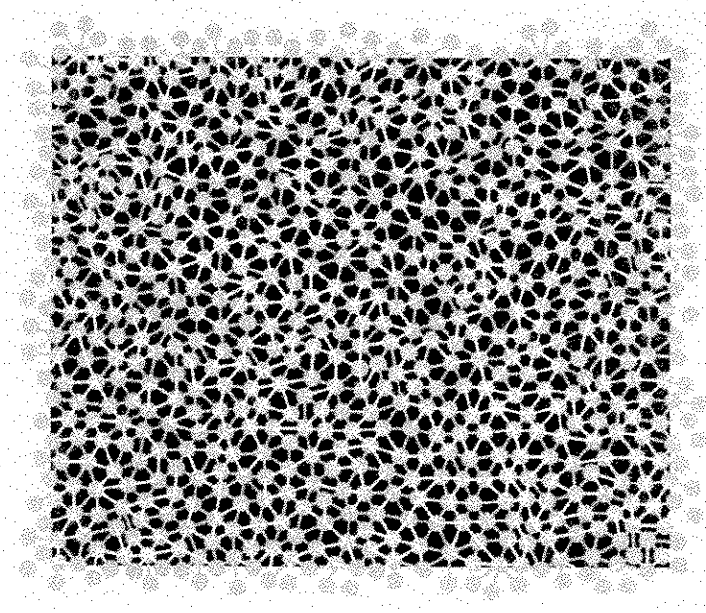

FIG. 15. Sample configuration of partially polymerized membrane with polymer bond fraction $p = 0.5$, viewed perpendicular to the membrane plane. The fluid bonds are gray, while the polymerized bonds are white.

Fig. 15, namely, $p_r = p_c = 2 \sin(\pi/18) = 0.35$ expected for triangulated networks in two dimensions. However, if the fluid bonds of Fig. 15 are completely removed and not replaced by polymerized bonds, thus leaving open holes in the membrane, then the membrane is floppier and p_r increases to about $\frac{2}{3}$, while p_c, of course, remains the same. The mixed-composition (fluid/polymerized) networks with no open holes have higher rigidity at a given polymerized bond concentration than the single-component (polymerized only) networks with holes because of the presence of isolated pockets of fluid that cannot diffuse past the polymerized regions. Single-component bond- or site-diluted networks have been studied in both two and three dimensions, and p_r is typically found to be d times p_c in the systems studied, where d is the embedding dimension (Thorpe, 1986).

Once the rigidity percolation threshold has been crossed from below p_r, the elastic moduli do not rise immediately to their values for a fully connected network. Rather, to a first approximation, the shear modulus rises linearly with $p - p_r$:

$$\mu(p)/\mu(p=1) = (p - p_r)/(1 - p_r) \text{ for } p > p_r, \quad (49a)$$
$$= 0 \text{ for } p < p_r, \quad (49b)$$

where, again, $p = 1$ for a fully polymerized network.

Both the mixed-composition and bond-depleted networks may be candidates to describe various partially polymerized networks. Consider the model erythrocyte cytoskeleton of Fig. 6, in which the chains represent the spectrin tetramers of the cytoskeleton and give the model network its elasticity [see Eq. (22)]. In some hereditary blood diseases, the erythrocytes have a lower spectrin concentration and may be examples of bond-diluted, single-component networks (but not mixed polymer/fluid networks since there is no trapped fluid component to the cytoskeleton). The shear modulus of these depleted cytoskeleta is found to decrease linearly as the spectrin content is reduced, as expected qualitatively from Eq. (49a). Although data are not available for highly depleted cytoskeleta (such cells are not viable), the extrapolated value for p_r is much lower than $p_r \sim \frac{2}{3}$ of a bond-depleted triangular network. This does not necessarily indicate that percolation theory is inapplicable to spectrin-depleted erythrocytes; it may be that the coordination of such cytoskeleta is still relatively uniform, but less than sixfold.

5.3 Defective Membranes in Three Dimensions

Bond-depleted networks in two dimensions possess reduced in-plane rigidity, as described in Sec. 5.2. When allowed to fluctuate out of plane into the third dimension, defective networks have fewer geometrical constraints and may adopt configurations in which one region of the membrane passes through a hole in another region. It is known that *phantom* polymerized membranes, in which the surface is free to intersect itself, are not flat but highly crumpled if $k_b = 0$ (see lectures by Nelson in Nelson *et al.*, 1989). Are bond-depleted membranes also crumpled?

The flatness characteristics of two types of bond-depleted (but otherwise self-avoiding) network have been investigated. In one case, bonds are randomly removed from a polymerized triangulated network, as described in the previous section on percolation. This type of network is observed to be flat for any $p > p_c$. In contrast, the geometry of a bond-depleted network known as a Sierpinski gasket is found to be described by the Flory exponent in Eq. (39).

A different defect structure is one in which network connectivity is uniform, but the interactions between junctions are variable. For example, the interaction strength or geometry of the intervertex potential might vary randomly across a network, corresponding to a glassy ground state. Simulation studies of systems with randomly varying interactions are challenging, because the network ground states are difficult to determine uniquely, and because many configurations must be sampled to construct accurate ensemble averages. Thus far, the temperature dependence of the membrane phases between the ground state and high-temperature configurations has not shown novel behavior in the limited studies of inhomogeneous networks with glassy ground states.

6. INTERACTIONS BETWEEN MEMBRANES

6.1 Interactions between Rigid Surfaces

The interactions of flexible membranes, particularly biological systems, involve forces of several different origins. Although this ar-

ticle focuses on effects arising from thermal fluctuations, it is important to appreciate the type and strength of chemical, entropic, and other components of membrane interactions. Here, we briefly review several features of the forces between rigid surfaces, before discussing the effects of undulations in Secs. 6.2 and 6.3. A more extensive treatment of these forces can be found in Israelachvili (1992).

6.1.1 van der Waals Forces Attractive, but relatively weak in strength, van der Waals forces may extend several nanometers away from a surface. The interaction arises from fluctuations in charge distributions at the atomic level: A quantum mechanical fluctuation that results in a dipole moment in one atom induces a dipole moment in a second atom. Thus, an attractive dipole–dipole interaction driven by fluctuations can be present between atoms with no permanent dipole moments. The van der Waals energy per unit surface area between two rigid surfaces with separation s decreases like s^{-2} at modest separations, and like s^{-4} at large separations.

6.1.2 Double-Layer Forces As introduced in Sec. 1.1, fluid membranes typically have a polar headgroup exposed to a polar solvent. Many polar groups can dissociate, leaving a charged region surrounded by counterions in the neighboring solvent, as illustrated in Fig. 16. In other situations, head groups may be capable of adsorbing ions from the solvent. Consequently, the membrane may carry a surface charge, which, together with the counterions in solution, constitute an electric double layer. Double-layer forces, which have been investigated theoretically and experimentally, are longer ranged than van der Waals forces, and are predominantly repulsive. The energy per unit surface area for the interaction between two double layers decays exponentially with separation.

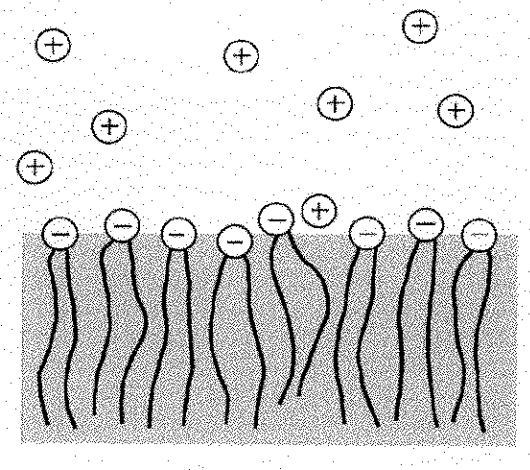

FIG. 16. Double layer at the boundary of a lipid monolayer with a solvent.

6.1.3 Hydration Forces The polar head groups of amphiphiles in a free biomembrane are surrounded by solvent molecules, which may be "bound" in the sense that the amphiphile and solvent have a strong mutual attraction. These solvent molecules must be removed if two membranes are to approach each other closely, suggesting that there is a repulsive hydration force associated with the hydrated amphiphile (the word "hydration" refers to water as a solvent). The pressure required to force bilayers together at small interlayer separation s is approximately exponential, $\exp(-s/s_0)$, and s_0 is found to be in the 1–3-nm range (Rand and Parsegian, 1989). The range of the hydration force is thus of the same magnitude as the attractive van der Waals force or repulsive thermal fluctuations of the bilayer itself.

6.1.4 Steric Interactions All of the above forces may apply to rigid or flexible membranes. However, flexible membranes also may undergo thermal fluctuations, resulting in a repulsive steric interaction between a rigid wall and a membrane or between membranes themselves. Membrane components, such as proteins, that extend into the solvent may give rise to additional steric interactions that are short-ranged compared to undulations but are more repulsive than undulations at small length scales.

The combined van der Waals and double-layer forces comprise the DLVO theory (Derjaguin and Landau, 1941; Verwey and Overbeek, 1948) of colloidal stability. As we have indicated, there may be several short-ranged interactions present in biomembranes in addition to the DLVO forces.

6.2 Entropic Repulsion of Fluctuating Membranes

The idea that membrane fluctuations result in repulsive interactions has support from several experimental observations:

1. vesicles composed of certain lipids show increased binding when their surfaces are under lateral tension;
2. in some situations, repulsion between lipid bilayers is reduced when one of the bilayers is attached to a rigid substrate; and
3. interbilayer repulsion may increase with temperature.

There are several fluctuation modes for a membrane, including out-of-plane undulations and fluctuations in membrane thickness. Here, we consider undulations, whose importance was pointed out by Helfrich (1978), and refer the interested reader to Israelachvili (1992) for a discussion of other fluctuation modes.

Consider a stack of n membranes as shown in Fig. 17, in which each membrane is taken to be parallel to the xy plane on average. A set of n functions is needed to describe the displacement of the membrane stack in the z direction. We label these functions $\psi_n(x,y)$ to show explicitly their x, y, and n dependence, and we assume that they are single valued as in the Monge representation. If the membranes are equally spaced on average, then

$$\int \psi_n(x,y)\, dxdy = ns, \tag{50}$$

where s is the average spacing between successive membranes and where the $n = 1$ membrane has an average height s above the xy plane. One can change the functions to regain a more familiar form by introducing a set of height functions $h_n(x,y)$

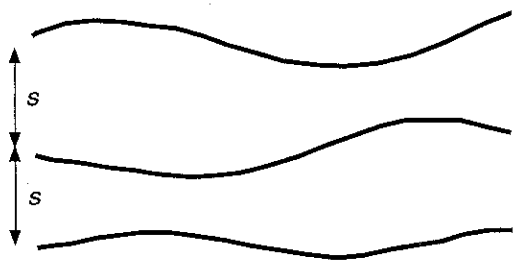

FIG. 17. Cross section through a membrane stack illustrating intermembrane repulsion arising from thermal fluctuations. The average separation between successive membranes is s.

$$h_n(x,y) = \psi_n(x,y) - ns, \tag{51}$$

such that $\int h_n(x,y)\, dxdy = 0$. For gentle undulations, the energy density of the membrane stack is

$$H = \int \left[(B/2) \sum_n (h_{n+1} - h_n)^2 + (k_b/2) \sum_n (h_{n,xx} + h_{n,yy})^2 \right] dxdy, \tag{52}$$

where $h_{n,xx} + h_{n,yy}$ is the mean curvature of the nth membrane and k_b is the bending modulus [see Eqs. (14) and (18)]. For notational simplicity, the xy arguments have been omitted from Eq. (52).

Compared to Eq. (18), the new feature of Eq. (52) is the elastic modulus B, which represents the intermembrane repulsion. Helfrich (1978) uses a self-consistent argument for obtaining B by (1) determining as a function of B the difference in the free energy per unit volume Δf_v between the many-membrane and single-membrane systems, and (2) imposing the elasticity relationship

$$B = s \frac{\partial^2 \Delta f_v}{\partial s^2}, \tag{53}$$

to the free energy found by procedure (1). This method yields (Safran, 1994)

$$B = 36/\pi^2 \beta^2 k_B s^4. \tag{54}$$

and a corresponding difference in the free energy per unit area $\Delta f_A = s\Delta f_v$ of

$$\Delta f_A = 3/\pi^2 \beta^2 k_B s^2. \tag{55}$$

There are two aspects of the free-energy expression in Eq. (55) worth noting. First, the s^{-2} dependence of the entropic repulsion is the same as that of the van der Waals interaction between rigid surfaces at moderate separations. Second, the repulsion increases with temperature. Both of these features are consistent with observations **1** and **2** listed at the beginning of this section. Helfrich (1978) estimates that the repulsion from undulations is about $\frac{1}{4}$ of the van der Waals interaction in magnitude for egg lecithin membranes.

A mean-field approach that avoids the introduction of the modulus B has been used

by Evans and Parsegian (1986) to obtain the undulation modes analogous to Eq. (42) and the free-energy density Δf_A. At large separations, their expressions have the same functional forms as those obtained by Helfrich and illustrate the substantial shift in the free-energy density across the 2–3-nm range in s arising from undulations.

6.3 Unbinding Transition

Fluctuations cause membranes to repel each other, and the magnitude of the repulsion increases with temperature. In principle, such fluctuations can overcome an attractive interaction between membranes that might be sufficient to bind them at low temperatures. Indeed, bilayer membranes have been observed to dissociate from a closely bound membrane stack over a very narrow temperature range (see Lipowsky in Lipowsky and Sackmann, 1995).

Since van der Waals interactions decrease more rapidly than s^{-2} at large separation s, then, for the purpose of investigating membrane binding, it is sufficient to use a square-well potential to represent the attractive interaction between two membranes:

$$V(s) = -U \text{ for } 0 < s < s_{max},$$
$$V(s) = 0 \text{ for } s > s_{max}, \tag{56}$$

where U and s_{max} are positive parameters that set the energy and length scales of the potential. At zero temperature, the membranes are confined to distances less than s_{max}, as dictated by Eq. (56). At temperatures greater than zero, the membranes repel but do not unbind until the transition temperature T^* given by

$$T^* \sim (k_b U s_{max}^2)^{1/2}, \tag{57}$$

which predicts that the more rigid the membranes or the stronger their attraction, the higher the unbinding temperature.

Systematic calculations have shown that the unbinding transition is continuous and that the mean separation diverges with temperature like $|T - T^*|^{-1}$ as the transition is approached from below T^*. For representative lipid bilayers, the estimated theoretical unbinding temperature varies by 50% about room temperature, depending on the membrane rigidity. Whether the suppression of thermal undulations is responsible for the tension-induced adhesion observed experimentally remains to be seen. Recent calculations, based on a description of the steric interaction that encompasses both the rigidity-dominated and tension-dominated regimes, show that the applied tension must be very large to permit tension-induced adhesion of fluid membranes (Seifert, 1995).

GLOSSARY

Cytoskeleton: A two- or three-dimensional protein network in a cell's interior.

Erythrocyte: A red blood cell; human erythrocytes are structurally simple since they do not have a nucleus and their cytoskeleton is connected only to the plasma membrane.

Fatty Acid: A carboxylic acid (-COOH) with a long hydrocarbon chain, found in natural fats and oils.

Fluid Membrane: Two-dimensional system with no resistance to in-plane shear.

Lipid: A small water-insoluble molecule with one or more hydrocarbon chains.

Lipid Bilayer: A double layer of oriented amphiphilic molecules; in biomembranes, the lipid bilayer is fluid.

Monolayer: A sheetlike structure with a thickness of one molecular unit.

Persistence Length: Length scale at which the relative orientation of chains or surfaces is uncorrelated.

Polymerized Membrane: Two-dimensional system with resistance to in-plane shear.

Protein: A macromolecule composed of one or more polypeptide chains (amino acids linked by peptide bonds); actin, spectrin, and tubulin are examples of proteins that form two- and three-dimensional networks in cells.

Works Cited

Alberts, B., Bray, D., Lewis, J., Raff, M., Roberts, K., Watson, J. D. (1989), *Molecular Biology of the Cell*, 2nd Ed., New York: Garland.

Boal, D. H. (1991), "Phases of attractive two-dimensional vesicles under pressure," *Phys. Rev. A* **43**, 6771–6777.

Derjaguin, B. V., Landau, L. (1941), *Acta Physicochim. URSS* **14**, 633–662.

Divigalpitiya, W. M. R., Frindt, R. F., Morrison, S. R. (1989), "Inclusion systems of organic molecules in restacked single-layer molybdenum disulphide," *Science* **246,** 369–371.

Evans, E. A., Parsegian, V. A. (1986), "Thermal-mechanical fluctuations enhance repulsion between bimolecular layers," *Proc. Natl. Acad. Sci. U.S.A.* **83,** 7132–7136.

Flory, P. J. (1953), *Principles of Polymer Chemistry,* Ithaca: Cornell University Press.

Fromherz, P., Röcker, C., Rüppel, D. (1986), "From discoid micelles to spherical vesicles: The concept of edge activity," *Faraday Discuss. Chem. Soc.* **81,** 39–48.

Fung, Y. C. (1994), *A First Course in Continuum Mechanics,* Englewood Cliffs, NJ: Prentice-Hall.

Gaines, G. L. Jr. (1966), *Insoluble Monolayers at Liquid-Gas Interfaces,* New York: Wiley.

Helfrich, W. (1978), "Steric interaction of fluid membranes in multilayer systems," *Z. Naturforsch.* **33a,** 305–315.

Israelachvili, J. N. (1992), *Intermolecular and Surface Forces,* 2nd Ed., New York: Academic.

Kroll, D. M., Gompper, G. (1992), "The conformation of fluid membranes: Monte Carlo simulations," *Science* **255,** 968–971.

Landau, L. D., Lifshitz, E. M. (1986), *Theory of Elasticity,* 3rd Ed., Oxford: Pergamon.

Le Doussal, P., Radzihovsky, L. (1992), "Self-consistent theory of polymerized membranes," *Phys. Rev. Lett.* **69,** 1209–1212.

Lipowsky, R., Sackmann, E. (Eds.) (1995), *Structure and Dynamics of Membranes,* Amsterdam: Elsevier.

Mohandas, N., Evans, E. (1994), "Mechanical properties of the red cell membrane in relation to molecular structure and genetic defects," *Annu. Rev. Biophys. Biomol. Struct.* **23,** 787–818.

Nelson, D., Piran, T., Weinberg, S. (Eds.) (1989), *Statistical Mechanics of Membranes and Surfaces,* Singapore: World Scientific.

Plischke, M., Boal, D. H. (1988), "Absence of a crumpling transition in strongly self-avoiding tethered membranes," *Phys. Rev. A* **38,** 4943–4945.

Rand, R. P., Parsegian, V. A. (1989), "Hydration forces between phospholipid bilayers," *Biochim. Biophys. Acta* **988,** 351–376.

Reif, F. (1965), *Fundamentals of Statistical and Thermal Physics,* New York: McGraw-Hill.

Ringsdorf, H., Schlarb, B., Venzmer, J. (1988), "Molecular architecture and function of polymeric oriented systems: models for the study of organization, surface recognition and dynamics of biomembranes," *Angew. Chem. Int. Ed. Engl.* **27,** 113–158.

Safran, S. A. (1994), *Statistical Thermodynamics of Surfaces, Interfaces and Membranes,* Reading, MA: Addison Wesley.

Seifert, U. (1995), "Self-consistent theory of bound vesicles," *Phys. Rev. Lett.* **74,** 5060–5063.

Thorpe, M. (1986), "Elastic properties of network glasses," *Ann. N. Y. Acad. Sci.* **484,** 206–213.

Verwey, E. J. W., Overbeek, J. Th. G. (1948), *Theory of Stability of Lyophobic Colloids,* Elsevier: Amsterdam.

Further Reading

de Gennes, P.-G. (1979), *Scaling Concepts in Polymer Physics,* Ithaca: Cornell University Press.

Gennis, R. B. (1989), *Biomembranes: Molecular Structure and Function,* New York: Springer-Verlag.

Gompper, G., Schick, M. (1994), "Self-assembling amphiphilic systems", in: C. Domb, J. L. Lebowitz (Eds.), *Phase Transitions and Critical Phenomena,* Vol. 16, New York: Academic.

Israelachvili, J. N. (1992), *Intermolecular and Surface Forces,* 2nd ed., New York: Academic.

Mouritsen, O. G. (1988), "Computer simulation of cooperative phenomena in lipid membranes," in: *Molecular Description of Biological Membrane Components by Computer-Aided Conformational Analysis,* Boca Raton, FL: CRC Press.

Nelson, D., Piran, T., Weinberg, S. (Eds.) (1989), *Statistical Mechanics of Membranes and Surfaces,* Singapore: World Scientific.

Safran, S. A. (1994), *Statistical Thermodynamics of Surfaces, Interfaces and Membranes,* Reading, MA: Addison Wesley.